J Mater Sci (2010) 45:1056–1064
DOI 10.1007/s10853-009-4042-2

In situ high-temperature X-ray and neutron diffraction of Cu–Mn oxide phases

Ping Wei · Mario Bieringer · Lachlan M. D. Cranswick · Anthony Petric

Received: 4 July 2009 / Accepted: 14 November 2009 / Published online: 1 December 2009

Abstract Copper–manganese oxides were analyzed by in situ high-temperature powder neutron and X-ray diffraction to investigate their crystal structure. Cu–Mn spinel was found to form a continuous solid solution with cubic symmetry between Mn_3O_4 and Cu_2MnO_4. A high-temperature phase with approximate composition $Cu_5Mn_4O_9$ was shown to have hexagonal symmetry. The cation distribution and lattice parameters of Cu–Mn spinel were resolved through Rietveld refinement of in situ neutron diffraction data. The results demonstrated that the Cu ion has a lower octahedral site preference than manganese ions, and quenching is not a reliable method to determine the equilibrium structure in the system.

Introduction

Copper–manganese oxides, $Cu_xMn_{3-x}O_4$, $Cu_{1-x}Mn_{1+x}O_2$, have interesting physical and catalytic properties [1–8]. For example, Cu–Mn oxide-based catalysts were proposed for the removal of air pollutants like carbon monoxide and nitrous oxides from exhaust gas [3, 9]. $Cu_xMn_{3-x}O_4$ spinel has high catalytic performance for steam reforming of methanol [7], and also exhibits high electrical conductivity ($\sim$200 S cm^{-1} at 800 °C). Its catalytic activity for oxygen reduction is comparable to that of lanthanum manganese perovskite, stoichiometric $CoFe_2O_4$, and Co_2MnO_4 spinel at intermediate temperature, which makes it a promising cathode material for solid oxide fuel cells [10]. Interesting physical and catalytic properties were expected in view of the presence of two Jahn–Teller ions in these materials, viz., Mn^{3+} and Cu^{2+}. In systems containing two types of Jahn–Teller ions, their interaction makes it difficult to predict the structure type as a function of temperature and Jahn–Teller ion concentration.

Sinha et al. [11] and Miyahara [12] reported that $CuMn_2O_4$ has the "normal" spinel structure with cubic symmetry. However, other authors reported that $CuMn_2O_4$ had tetragonal structure when prepared by quenching from temperatures between 750 and 940 °C [13, 14]. Dubrovina et al. [15] studied the $Cu_xMn_{3-x}O_4$ system through high-temperature X-ray diffraction (XRD), and found that samples with $x = 0.5$, 0.75, and 1.0 have the cubic spinel structure at 900 °C in air. However, quenching in air gave rise to tetragonal distortion with $c/a > 1$ [16], consistent with the previous result on quenched samples [6, 9, 14, 17].

Driessens and Rieck [18] investigated the interaction of copper and manganese oxides in air between 750 and 1400 °C and reported $Cu_{1+x}Mn_{1-x}O_2$ to be a crednerite-like phase with monoclinic structure ($0 < x < 0.06$) and a delafossite-like phase with hexagonal structure ($0.08 < x < 0.12$). At 1060 ± 10 °C, the delafossite structure was reported to decompose. Trari et al. [8] reported that solid solutions of $Cu_{1+x}Mn_{1-x}O_2$ have monoclinic crednerite structure (space group $C2/m$), and a very narrow composition range ($0.1 \leq x \leq 0.15$).

Inconsistencies regarding the crystal structure of Cu–Mn oxides might arise from the fact that most experiments depended on the measurements of quenched samples. The

P. Wei · A. Petric (✉)
Department of Materials Science and Engineering, McMaster University, Hamilton, ON, Canada
e-mail: petric@mcmaster.ca

M. Bieringer
Department of Chemistry, University of Manitoba, Winnipeg, MB, Canada

L. M. D. Cranswick
Canadian Neutron Beam Centre, National Research Council Canada, Chalk River Laboratories, ON, Canada

quenching cannot prevent changes of crystal symmetry. Therefore, investigation of the cation distribution in Cu–Mn spinel through quenching leaves some doubt about the crystal structure of the materials at high temperatures [9, 19–22]. In situ measurement at high temperature is necessary to clarify the crystal structure of Cu–Mn oxides. Neutron diffraction is an appropriate technique to obtain the precise Cu and Mn ion distribution and other crystallographic parameters aided by Rietveld structure refinement as Cu and Mn have neutron scattering lengths of opposite sign [b(Cu) = 0.76×10^{-12}, b(Mn) = -0.36×10^{-12} cm] [23]. In this study, a combination of in situ X-ray and in situ neutron diffraction was used to determine the structure of Cu–Mn oxides at high temperatures.

Experimental

Samples for in situ high-temperature neutron and XRD measurements were prepared from CuO (99.7%, 200 mesh, Alfa Aesar, Ward Hill, MA, USA) and MnO_2 (99.9%, 325 mesh, Alfa Aesar) through solid-state reaction. Stoichiometric amounts of the oxides were mixed in a Nalgene container. In order to achieve intimate mixing of the constituent oxides, the powders were ball-milled in 100% anhydrous ethanol with 5 mm diameter yttria-stabilized zirconia balls (TOSOH USA, Inc., Grove City, OH, USA). Pure ethanol was added to facilitate mixing and flowing of the powder out of the container after mixing. Milling of powders was performed for 24 h. After milling, the powders were transferred to porcelain dishes and heated to 353 K on a hot plate to evaporate the ethanol.

During pressing, a cylindrical die was used and uniaxial pressing was performed on a manually operated press (Model K, F.S. Carver Inc., Summit, NJ, USA) to form the green body. The pressure was maintained around 80–100 MPa. No organic binder was used during the process. The pressed samples were annealed at different temperatures in order to obtain pure spinel. The annealing temperatures and time were based on available data for the Cu–Mn–O phase diagram [6, 9], and are given in Table 1. The samples were heated to the corresponding annealing temperatures at a heating rate of 5 °C/min. After annealing, they were quenched to room temperature in air and ground into powder for XRD measurements. The phase content was determined by a Bruker D8 Advanced X-ray diffractometer with Cu$K\alpha_1$ radiation (germanium monochromator). Diffraction patterns were acquired within the 2θ range from 15° to 65° with a step time of 5–10 s.

For in situ high-temperature neutron diffraction measurements, the powders were put into quartz tubes. The tubes were sealed with a reduced pressure of air inside to maintain a pressure near one atmosphere during high-temperature testing. In situ neutron diffraction was performed at the Canadian Neutron Beam Centre, NRC, Chalk River, on the C2 Spectrometer equipped with a silicon monochromator [X, Y] [24, 25]. Diffraction patterns were acquired for $0° < 2\theta < 120°$ using two different wavelengths: 1.32927(6) and 2.37083(13) Å. Rietveld refinement was performed using EXPGUI, a graphical user interface for GSAS [26, 27]. The stage temperature was controlled by type K thermocouples and the accuracy is ±2.2 °C. There were thermocouples at the top and bottom of the quartz tubes, and the average value of them was taken as the sample temperature. The maximum temperature difference between two thermocouples is 10 °C during the in situ neutron diffraction measurements.

The in situ powder XRD data were measured at the University of Manitoba with a PANalytical X'Pert Pro System using $K\alpha_{1,2}$ radiation equipped with a diffracted beam Ni-filter and an X'Celerator detector. The samples were cast as thin layers directly onto the Pt heating element on an HTK-2000 (Anton Paar USA, Inc., Ashland, VA, USA) furnace attachment. The temperature of the HTK-2000 heating stage is accurate within ±5 up to 1200 °C. The powder diffraction data sets were measured at 0.0167° steps with 50 s per step counting times covering the 2θ range from 10° to 70°. The samples were typically heated to the initial annealing temperature and measured 10 times for 25 min each before raising or lowering the temperature by 25 °C. The last data set at each temperature were analyzed by EVA phase identification software based on the PDF-2 2003 database (ICDD, Newtown Square, PA, USA) at McMaster University.

The composition of the samples was analyzed by a Varian VISTA-PRO CCD simultaneous inductively coupled plasma optical emission spectrometry (ICP-OES). It is clear that the compositions of the powder samples were adequately controlled (Table 2).

Table 1 Preparation of the samples for neutron diffraction and XRD measurements

Nominal composition	Cu/(Cu + Mn) (mole)	Annealing temperature (°C)	Time (days)
$Cu_{0.8}Mn_{2.2}O_4$	0.27	900	3
$Cu_{1.0}Mn_{2.0}O_4$	0.33	850	3
$Cu_{1.1}Mn_{1.9}O_4$	0.37	790	4
$Cu_{1.3}Mn_{1.7}O_4$	0.43	690	5

Table 2 Composition analysis of the powders by ICP

Sample	Cu	Mn
$Cu_{0.8}Mn_{2.2}O_4$	0.803	2.197
$Cu_{1.0}Mn_{2.0}O_4$	1.007	1.993
$Cu_{1.1}Mn_{1.9}O_4$	1.108	1.892
$Cu_{1.3}Mn_{1.7}O_4$	1.309	1.691

Results and discussion

XRD measurement of quenched samples

Room temperature XRD measurements of the samples quenched from temperatures in the spinel stability range are shown in Figs. 1 and 2. It can be seen that the samples with nominal compositions of $Cu_{0.8}Mn_{2.2}O_4$ and $Cu_{1.0}Mn_{2.0}O_4$ have tetragonal symmetry, and other spinel compositions have cubic structure after quenching.

In situ high-temperature XRD measurements

The phase characterization shows that the spinel maintains cubic structure throughout the temperature range for three samples (Fig. 3). For $Cu_{1.1}Mn_{1.9}O_4$, single spinel exists in the temperature range 700–825 °C. Below 700 °C, the cubic spinel and Mn_2O_3 coexist. As the temperature increases above 950 °C, $CuMnO_2$, which is isomorphous with that of rhombohedral $CuRhO_2$ (space group : $R\bar{3}m(166)$), forms and the amount of this phase increases with temperature. Meanwhile, the fraction of cubic spinel in the sample decreases markedly (Fig. 4). The cubic spinel phase fraction begins to increase again after 1100 °C, which signals the limit of stability of $CuMnO_2$ and its transformation to spinel. For $Cu_{0.8}Mn_{2.2}O_4$, the temperature range of single phase spinel is 775–975 °C. Below 775 °C, the phases are cubic spinel and Mn_2O_3. As the temperature increases above 975 °C, the formation of rhombohedral $CuMnO_2$ is observed (Fig. 4). Above 1125 °C, $CuMnO_2$ disappears, leaving only single phase spinel with cubic symmetry. For $Cu_{1.3}Mn_{1.7}O_4$, single spinel phase exists within the range 425–575 °C. Above this temperature range, spinel coexists with CuO, whereas below, Mn_2O_3 appears.

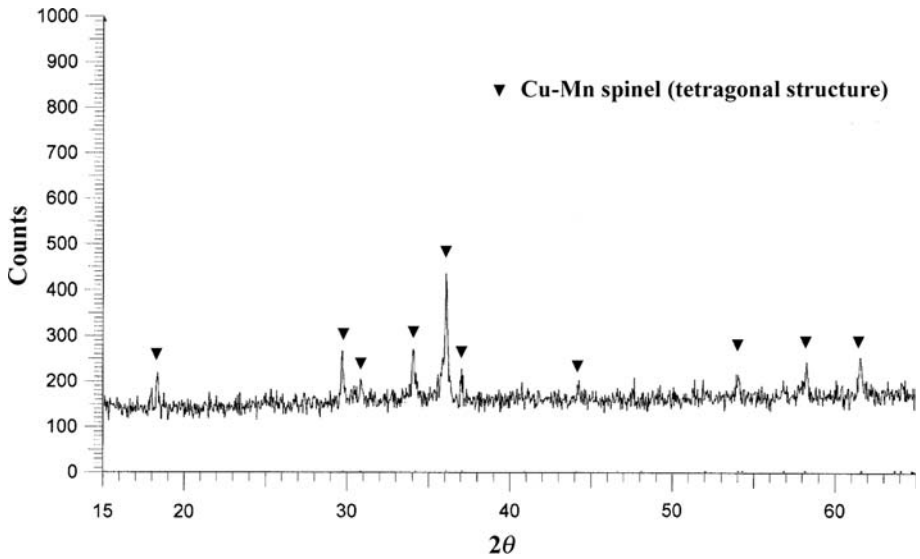

Fig. 1 X-ray pattern showing tetragonal symmetry for $Cu_{0.8}Mn_{2.2}O_4$ and $Cu_{1.0}Mn_{2.0}O_4$ (based on quenched samples)

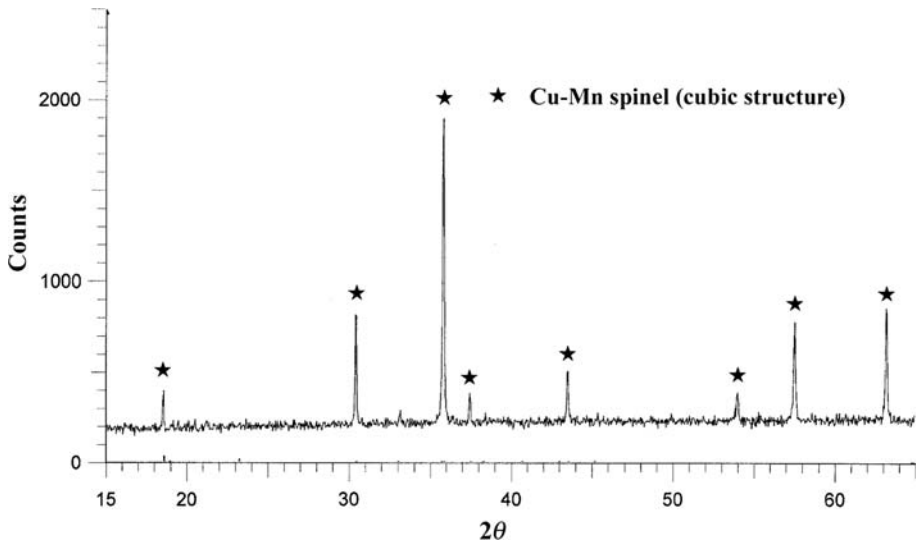

Fig. 2 X-ray pattern showing cubic symmetry for $Cu_{1.1}Mn_{1.9}O_4$ and $Cu_{1.3}Mn_{1.7}O_4$ (based on quenched samples)

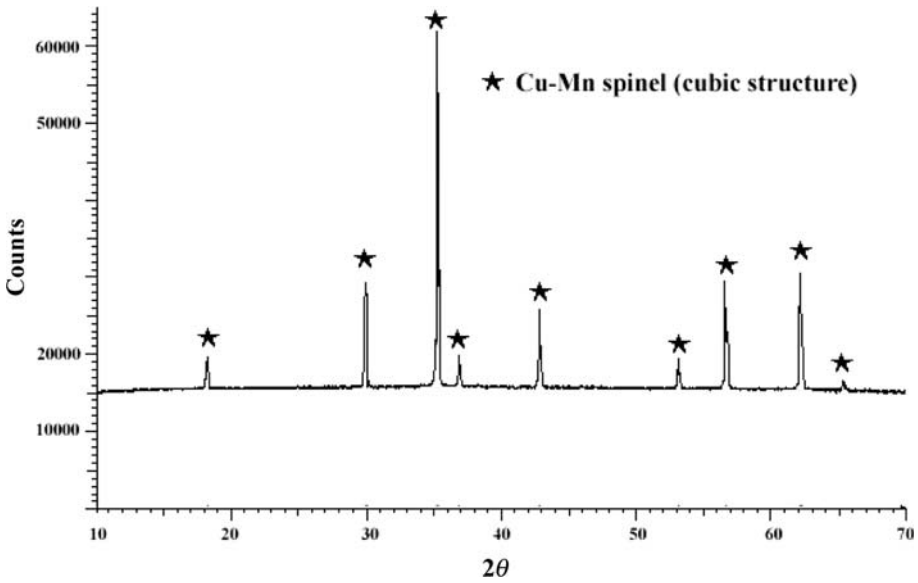

Fig. 3 In situ high-temperature XRD of Cu–Mn spinel (taken after in situ high-temperature neutron diffraction)

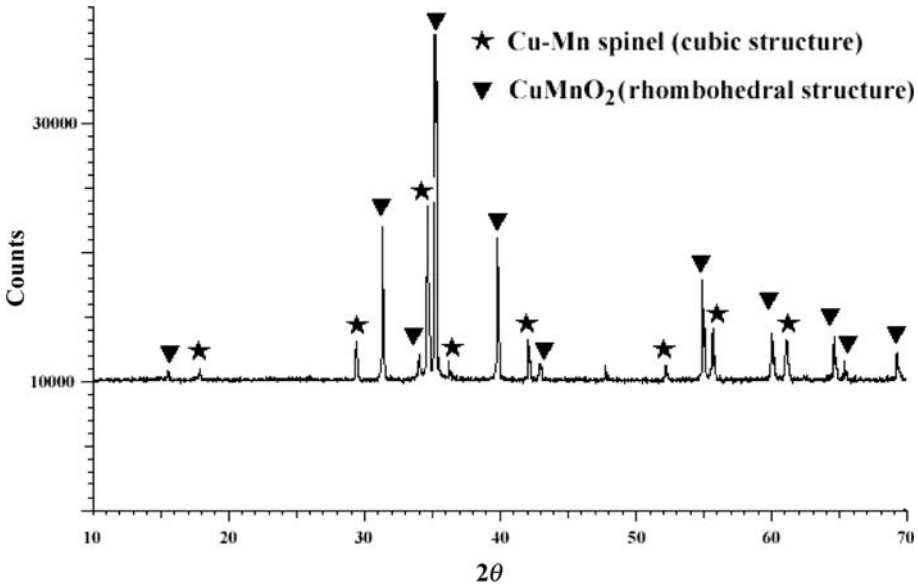

Fig. 4 In situ high-temperature XRD of $CuMnO_2$ and Cu–Mn spinel (taken after in situ high-temperature neutron diffraction)

The spinel boundaries from in situ high-temperature XRD data based on the samples of $Cu_{0.8}Mn_{2.2}O_4$ and $Cu_{1.1}Mn_{1.9}O_4$ matched closely with the mid-composition investigation of Vandenberghe and Robbrecht [6], whereas for $Cu_{1.3}Mn_{1.7}O_4$, there is only partial agreement. This difference could be due to a failure to reach equilibrium for the sample at temperatures below 750 °C. The results are summarized by a Cu–Mn–O phase diagram modeled using FACTSage software and based on the in situ high-temperature XRD and neutron diffraction measurements (Fig. 5). High-temperature measurements show that Cu–Mn spinel has cubic symmetry over the composition range tested. However, samples $Cu_{0.8}Mn_{2.2}O_4$ and $Cu_{1.0}Mn_{2.0}O_4$ exhibited tetragonal symmetry after quenching (Fig. 1). At $x > 1.0$ in $Cu_xMn_{1-x}O_4$, the spinel showed cubic symmetry after quenching (Fig. 2), which is consistent with the literature [6, 15]. We may conclude that the presence of tetragonal spinel observed in early studies was due to the failure of quenching to maintain the equilibrium structure.

Trari et al. [8] proposed that above 1150 °C, the following reaction occurs:

$$Cu_{1+x}Mn_{1-x}O_2 \rightarrow Cu_yMn_{3-y}O_4(\text{spinel}) + \text{liquid} \quad (1)$$

Our results from $Cu_{0.8}Mn_{2.2}O_4$ show that up to 1125 °C, the stable phases are rhombohedral $CuMnO_2$ and cubic $Cu_xMn_{3-x}O_4$ spinel. The lattice constants of $CuMnO_2$ are shown in Table 3. $CuMnO_2$ disappeared and the single spinel phase remained at temperatures above 1125 °C. This is consistent with the results of Trari el al. [8]. Liquid phase should also exist above this temperature, but cannot be

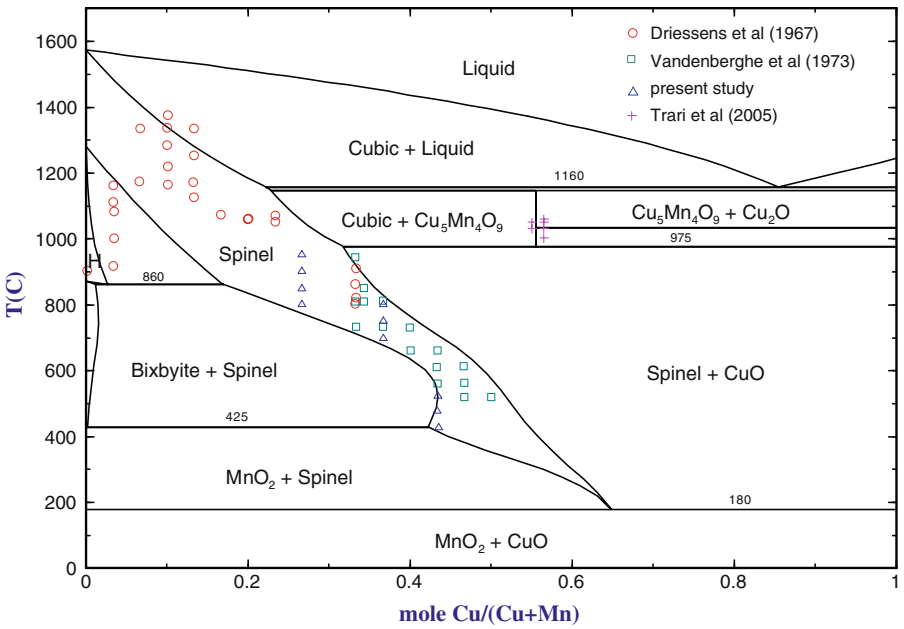

Fig. 5 Cu–Mn–O phase diagram from FACTSage modeled by the compound energy formalism

Table 3 Lattice constants of $CuMnO_2$

Lattice constant					
a (Å)	*b* (Å)	*c* (Å)	α	β	γ
3.074	3.074	17.119	90°	90°	120°

detected by XRD. The in situ high-temperature X-ray measurements of $CuMnO_2$ did not detect monoclinic symmetry at the temperatures up to 1150 °C. Apparently, the monoclinic distortion found by Trari et al. [8] was a consequence of quenching, leading to decreased cell symmetry. The distortion could be caused by the presence of Jahn–Teller ions, e.g., Mn^{3+}, which form on octahedral sites and increase the degree of distortion. In order to contain these Jahn–Teller ions during cooling, the cell tends to elongate along the *c*-axis and results in tetragonal distortion. At high temperatures, as the lattice expands, distortion is not necessary to accommodate these Jahn–Teller ions and cubic symmetry can be maintained.

The transformation between cubic and tetragonal symmetry at *x* near 1.0 in $Cu_xMn_{3-x}O_4$ solid solutions, reported in the literature [6], was not observed by the in situ X-ray measurements, in agreement with the in situ neutron measurements. All the $Cu_xMn_{3-x}O_4$ solid solutions showed cubic symmetry at high temperatures. It was demonstrated that $CuMnO_2$ is unstable at 1150 °C. This is quite consistent with previous results [8, 18]. In situ high-temperature XRD measurements show that $CuMnO_2$ at high temperatures has rhombohedral structure, not monoclinic, contrary to earlier literature.

In situ high-temperature neutron diffraction measurements

The cation distribution and lattice parameters of the spinels based on Rietveld refinement using a model with $Fd\bar{3}m$ space group are shown in Tables 4 and 5. In the tables, R_p is the profile *R*-factor and wR_p is the weighted profile *R*-factor.

The change of lattice parameters of the spinel with temperature is shown in Figs. 6 and 7. It can be seen that the cubic lattice parameter of the spinel phase increases with temperature, and decreases with increasing Cu content in $Cu_xMn_{3-x}O_4$ solid solutions. Vandenberghe and Robbrecht [6] also observed that the lattice parameter diminished with increasing *x* in $Cu_xMn_{3-x}O_4$ solid solutions. They proposed that the copper ions distribute in a certain ratio over the octahedral and tetrahedral sublattices, and the lattice parameter decreased with increasing tetrahedral copper concentration.

The cation distribution from our refinement confirmed this hypothesis. Copper ions occupy more tetrahedral sites than octahedral sites in $Cu_xMn_{3-x}O_4$ solid solutions (Fig. 8). As ionic radii of Cu^+ and Cu^{2+} on tetrahedral sites are smaller than that of Mn^{2+} on the same sites [28], the lattice parameter decreases when copper ions replace manganese ions on tetrahedral sites. In situ neutron diffraction results confirm the findings of in situ XRD that $Cu_xMn_{3-x}O_4$ spinel has cubic structure at high temperatures. Mn_3O_4 at intermediate temperatures has tetragonal structure and the cation distribution of $(Mn^{2+})[Mn^{3+}Mn^{3+}]O_4$ was proposed for this symmetry [29]. Here, round brackets mean tetrahedral sites and square brackets octahedral sites. It is reasonably deduced that as

Table 4 Cation distribution in the spinel phase

Samples	Cu/(Cu + Mn) (mole)	Temperature (°C)	Occupancy at tetrahedral sites		Occupancy at octahedral sites	
			Cu	Mn	Cu	Mn
$Cu_{0.8}Mn_{2.2}O_4$	0.27	698	0.561(6)	0.439(6)	0.101(6)	0.899(6)
		798	0.54(1)	0.46(1)	0.12(1)	0.88(1)
		898	0.548(6)	0.452(6)	0.112(6)	0.888(6)
		998	0.52(1)	0.48(1)	0.11(1)	0.89(1)
$Cu_{1.0}Mn_{2.0}O_4$	0.33	746	0.663(8)	0.337(8)	0.150(8)	0.850(8)
		796	0.655(7)	0.345(7)	0.117(7)	0.883(7)
		846	0.655(4)	0.345(4)	0.126(4)	0.874(4)
		946	0.653(4)	0.347(4)	0.132(4)	0.868(4)
$Cu_{1.1}Mn_{1.9}O_4$	0.37	646	0.739(8)	0.261(8)	0.150(8)	0.850(8)
		696	0.733(6)	0.267(6)	0.134(6)	0.866(6)
		786	0.712(8)	0.288(8)	0.145(3)	0.855(3)
		895	0.70(1)	0.30(1)	0.150(6)	0.850(6)
		945	0.692(7)	0.308(7)	0.140(7)	0.860(7)
$Cu_{1.3}Mn_{1.7}O_4$	0.43	25	0.877(7)	0.123(7)	0.134(5)	0.866(5)
		548	0.853(9)	0.147(9)	0.150(9)	0.850(9)
		598	0.834(9)	0.166(9)	0.160(6)	0.840(6)
		688	0.834(7)	0.166(7)	0.170(3)	0.830(3)
		797	0.859(9)	0.141(9)	0.179(7)	0.821(7)
		847	0.855(9)	0.145(9)	0.169(8)	0.831(8)

Table 5 Lattice parameters of the spinel phase

Sample	Cu/(Cu + Mn) (mole)	Temperature (°C)	Spinel, cubic ($a = b = c$ (Å))	x in $Cu_x Mn_{3-x}O_4$ spinel	R_p	wR_p
$Cu_{0.8}Mn_{2.2}O_4$	0.27	698	8.470	0.763	0.0481	0.0624
		798	8.488	0.78	0.0476	0.0613
		898	8.494	0.772	0.05	0.0635
		998	8.509	0.74	0.0477	0.0617
$Cu_{1.0}Mn_{2.0}O_4$	0.33	746	8.446	0.963	0.0528	0.0671
		796	8.459	0.889	0.055	0.073
		846	8.470	0.907	0.056	0.0747
		946	8.481	0.917	0.0515	0.0663
$Cu_{1.1}Mn_{1.9}O_4$	0.37	646	8.429	1.039	0.056	0.0716
		696	8.434	1.001	0.0521	0.0675
		786	8.448	1.002	0.05	0.0641
		895	8.465	1.00	0.054	0.0701
		945	8.467	1.039	0.0541	0.07
$Cu_{1.3}Mn_{1.7}O_4$	0.43	25	8.336	1.145	0.0593	0.0756
		548	8.392	1.153	0.0584	0.075
		598	8.401	1.154	0.0571	0.0738
		688	8.422	1.174	0.0573	0.0737
		797	8.430	1.217	0.0635	0.0801
		847	8.44	1.193	0.0587	0.0746

copper is added to Mn_3O_4, the cubic phase is stabilized to lower temperatures and the change in lattice stability might be related to a change in ionic configuration. Dubrovina et al. [15] studied $Cu_xMn_{3-x}O_4$ solid solutions with compositions of $0.5 \leq x \leq 1.0$ at 900 °C in air through in situ XRD and also found that $Cu_xMn_{3-x}O_4$ solid solutions had cubic structure at high temperature, but quenching in air gave rise to tetragonal distortion, which was consistent

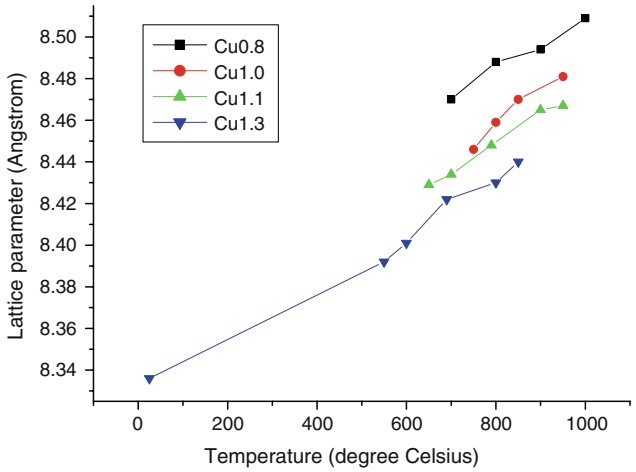

Fig. 6 Lattice parameter of the spinel as a function of temperature

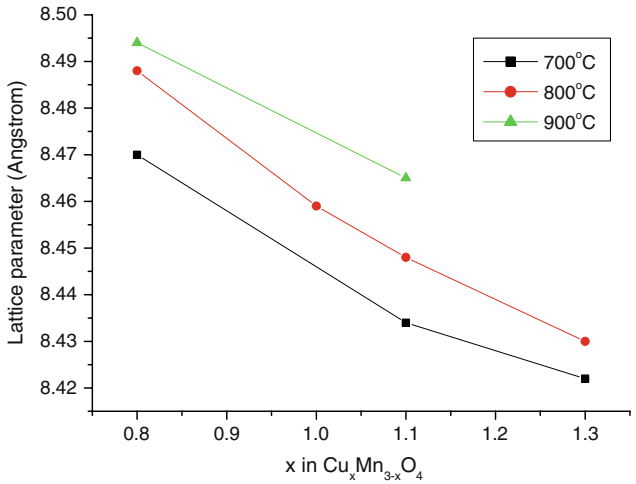

Fig. 7 Lattice parameter of the spinel as a function of x in $Cu_xMn_{3-x}O_4$

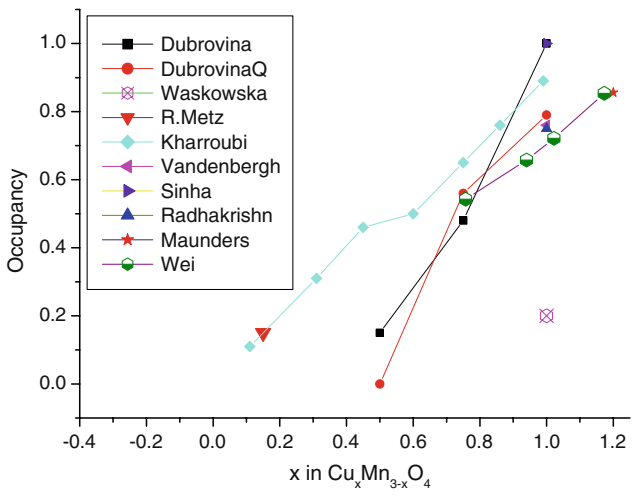

Fig. 8 Fraction of copper cations on tetrahedral sites of $Cu_xMn_{3-x}O_4$

with our experiments for $Cu_{0.8}Mn_{2.2}O_4$ and $Cu_{1.0}Mn_{2.0}O_4$ (Fig. 1). It seems that quenching cannot prevent a change in crystal symmetry of $Cu_xMn_{3-x}O_4$ spinel, and is not a reliable way to determine equilibrium structure in this system. Over 40 years ago, Levin and Roth found that the high-temperature phases in the bismuth oxide system detected by high-temperature XRD were different from those measured in the cooled samples, and concluded that in situ studies of high-temperature phases were necessary for studying that system [30]. Clearly, the same conclusion applies to Cu–Mn–O system.

Different cation distributions have been proposed for $Cu_xMn_{3-x}O_4$ spinel (Table 6). The results from our in situ high-temperature neutron measurements were compared with those of others (Figs. 8 and 9). The label of 'Wei' in the legend represents the present data from our experiments. As cation distributions in $Cu_xMn_{3-x}O_4$ spinel did not show significant variation at intermediate temperatures (Table 4), average values were taken for comparison. Symbols of 'Dubrovina' and 'DubrovinaQ' in the figures mean the data from in situ and room temperature measurements based on quenched samples [15]. It can be seen that the cation distributions from Maunders et al. [31], Dubrovina et al. [15], Radhakrishnan and Biswas [22], and Vandenberghe et al. [23] matched with ours better than others. Although the cation distributions in $CuMn_2O_4$ from Vandenberghe et al. [23] and Radhakrishnan and Biswas [22] are consistent with each other, the ionic configurations they proposed are quite different (Table 6). The in situ neutron diffraction measurements show that the sample with nominal composition $Cu_{1.1}Mn_{1.9}O_4$ and a refined composition $Cu_{1.00}Mn_{2.00}O_4$ had a cation distribution of $(Cu_{0.70}Mn_{0.30})[Cu_{0.30}Mn_{1.70}]$ at 895 °C (Table 4). It is clear that quenching can freeze the cation distribution in $Cu_xMn_{3-x}O_4$ spinel from high temperature to room temperature in some cases. However, caution must be taken when using quenched samples to study the structure of the materials, as most of the data from quenching experiments deviate significantly from in situ measurements.

From previous neutron diffraction data on the cation distribution in $CuMn_2O_4$ [14, 22, 32], it follows that Cu ions have a lower octahedral site preference than manganese ions. Our experiments also found more Cu ions on tetrahedral sites than on octahedral sites. Figure 10 shows that at intermediate temperatures, the concentration of copper ions on tetrahedral sites is much higher than that on octahedral sites. Moreover, the former increases with increasing x in $Cu_xMn_{3-x}O_4$ more quickly than the latter. The concentration of manganese ions on tetrahedral and octahedral sites decreases with increasing copper concentration. Vandenberghe et al. [6, 21] proposed the

Table 6 Cation distributions in $Cu_xMn_{3-x}O_4$

Reference	x in $Cu_xMn_{3-x}O_4$	Cation distributions
Maunders et al. [31]	1.2	$(Cu^{2+}_{0.856}Mn^{2+}_{0.144})\,[Cu^{2+}_{0.344}Mn^{3+}_{0.666}Mn^{4+}_{0.99}]$ quenched
Dubrovina et al. [15]	0.5	$(Mn^{2+}_{0.85}Cu^{+}_{0.15})\,[Cu^{2+}_{0.35}Mn^{3+}_{1.15}Mn^{4+}_{0.50}]$ at 900 °C $(Mn^{2+}_{1.0})\,[Cu^{2+}_{0.51}Mn^{3+}_{0.98}Mn^{4+}_{0.51}]$ quenched
	0.75	$(Mn^{2+}_{0.52}Cu^{+}_{0.25}Cu^{2+}_{0.23})\,[Cu^{2+}_{0.27}Mn^{3+}_{1.21}Mn^{4+}_{0.52}]$ at 900 °C
		$(Mn^{2+}_{0.44}Cu^{+}_{0.25}Cu^{2+}_{0.31})\,[Cu^{2+}_{0.19}Mn^{3+}_{1.37}Mn^{4+}_{0.44}]$ quenched
	1.0	$(Cu^{+}_{1.0})\,[Mn^{3+}_{1.01}Mn^{4+}_{0.99}]$ at 900 °C $(Mn^{2+}_{0.21}Cu^{2+}_{0.79})\,[Cu^{2+}_{0.21}Mn^{3+}_{1.58}Mn^{4+}_{0.21}]$ quenched
Waskowska et al. [2]	$x = 1$	$(Cu^{+}_{0.2}Mn^{2+}_{0.8})\,[Cu^{2+}_{0.8}Mn^{3+}_{0.2}Mn^{4+}_{1.0}]$
Metz [33]	$0 \le x < 0.3$	$(Cu^{+}_{x}Mn^{2+}_{1-x})\,[Mn^{3+}_{2-x}Mn^{4+}_{x}]$ quenched
	$0.3 \le x < 1.0$	$\left(Cu^{+}_{x-y}Mn^{2+}_{1-x+y}\right)\left[Cu^{2+}_{y}Mn^{3+}_{2-x-y}Mn^{4+}_{x}\right]$ quenched
Kharroubi et al. [17]	$x < 0.6$	$(Cu^{+}_{x}Mn^{2+}_{1-x})\,[Mn^{3+}_{2-x}Mn^{4+}_{x}]$ quenched
	$1.0 > x > 0.6$	$\left(Cu^{+}_{x-y}Mn^{2+}_{1-x+y}\right)\left[Cu^{2+}_{y}Mn^{3+}_{2-x-y}Mn^{4+}_{x}\right]$ [a] quenched
Radhakrishnan and Biswas [22]	$x = 1$	$(Cu^{2+}_{0.50}Cu^{+}_{0.25}Mn^{3+}_{0.25})\,[Cu^{2+}_{0.25}Mn^{3+}_{1.50}Mn^{4+}_{0.25}]$ quenched
Vandenberghe et al. [23]	$x = 1$	$(Cu^{+}_{0.76}Mn^{3+}_{0.24})\,[Cu^{2+}_{0.24}Mn^{3+}_{1.0}Mn^{4+}_{0.76}]$ quenched $(Cu^{+}_{0.76}Mn^{2+}_{0.24})\,[Cu^{2+}_{0.24}Mn^{3+}_{0.76}Mn^{4+}_{1.0}]$ quenched
Sinha et al. [11]	$x = 1$	$(Cu^{+})\,[Mn^{3+}Mn^{4+}]$

[a] y represents a low value (<0.20), and is taken as 0.1 in our calculations

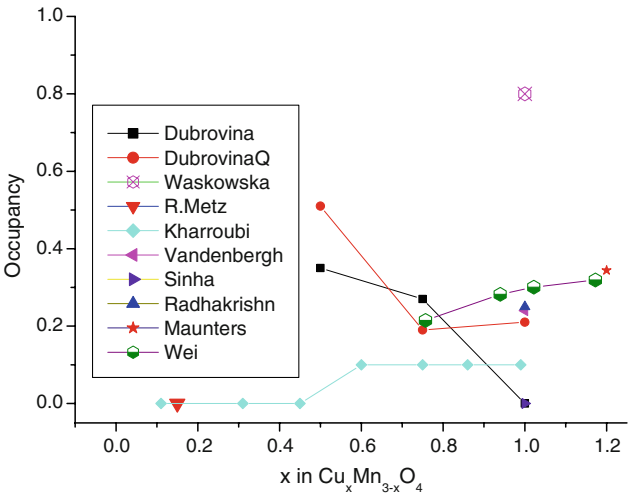

Fig. 9 Fraction of copper cations on octahedral sites of $Cu_xMn_{3-x}O_4$

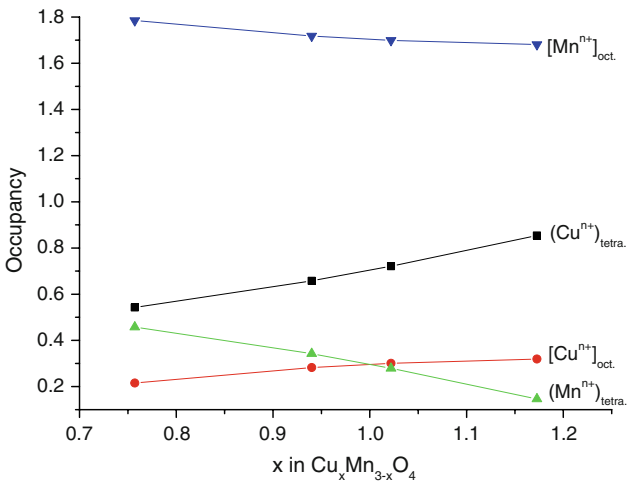

Fig. 10 Cation distribution in $Cu_xMn_{3-x}O_4$ from in situ neutron diffraction

following exchange reaction based on neutron diffraction measurements:

$$Cu_{tetra} + Mn_{oct} \Leftrightarrow Cu_{oct} + Mn_{tetra} \quad (2)$$

which shifts to the right at high temperatures. From Table 4, it can be seen that for $Cu_{1.3}Mn_{1.7}O_4$, $(Cu^{n+})_{tetra}$ and $[Mn^{n+}]_{oct}$ decrease, whereas $[Cu^{n+}]_{oct}$ and $(Mn^{n+})_{tetra}$ increase as temperature increases from room temperature to high temperature, which demonstrates that reaction (2) proceeds to the right as temperature increases. Many models have been proposed for the cation distribution, but there is no clear consensus which one is more accurate [2, 6, 11, 14, 22, 29, 33]. Clearly, the site exchange based on Eq. 2 during quenching is not significant as the cation distribution from quenched samples was similar to the in situ diffraction measurements in some cases [15, 22, 23, 31], but the crystal symmetry may change with temperature or composition. Dubrovina et al. [15] stated that the competing cooperative effects of the Jahn–Teller ions on tetrahedral and octahedral sublattices play a decisive role in determining the structure of the spinel in the absence of thermal disordering. At high temperatures, the thermal factor may be assumed to play a key role in determining the equilibrium state of $Cu_xMn_{3-x}O_4$ solid solutions.

Waskowska et al. [2] mentioned that the amount of distorting ions is the key to crystal symmetry in $Cu_xMn_{3-x}O_4$. The critical fraction of distortive ions on octahedral sites should be about 55%. It can be seen that these explanations are inconsistent, but both agreed that the Jahn–Teller ions play a key role on crystal symmetry of Cu–Mn spinel.

The compositions of the cubic spinel can be calculated based on the refined distribution for manganese and copper as well as the site multiplicity for tetrahedral and octahedral sites following the equation: $Cu_{total} = Cu_{tet} + Cu_{octa}$. It can be seen that the compositions of the samples based on refinement (Table 5) are quite different from ICP analysis (Table 2). The explanation is that ICP analysis gives compositions of the whole sample, not a specific phase, while the compositions obtained from refinement is for cubic spinel only.

Conclusions

In situ XRD and neutron diffraction measurements reveal that $Cu_xMn_{3-x}O_4$ spinel has cubic structure from $x = 0.8$ to 1.4 at high temperatures. $CuMnO_2$ with rhombohedral structure was detected at high temperatures, and monoclinic symmetry at the temperatures up to 1100 °C was not observed in the in situ high-temperature XRD measurements. Clearly, quenching normally decreases cell symmetry of Cu–Mn oxides, and is not a reliable way to determine equilibrium structure in the Cu–Mn–O system. Cation distributions from refinement of in situ high-temperature neutron diffraction data show that the cubic lattice parameter of the spinel phase increases with temperature, and decreases with increasing Cu content in $Cu_xMn_{3-x}O_4$ solid solutions. Manganese has a greater tendency to occupy octahedral sites, leaving more copper on tetrahedral sites.

Acknowledgements We wish to thank the Natural Sciences and Engineering Research Council of Canada for financial support. The authors also acknowledge I. David Brown, James Britten, Shahab Derakhshan, and Wenhe Gong for their assistance in this study.

References

1. Bessekhouad Y, Gabes Y, Bouguelia A, Trari M (2007) J Mater Sci 42:6469. doi:10.1007/s10853-006-1250-x
2. Waskowska A, Gerward L, Olsen JS, Steenstrup S, Talik E (2001) J Phys Condens Matter 13:2549
3. Fierro G, Ferraris G, Dragone R, Jacono LL, Faticanti M (2006) Catal Today 116:38
4. Gillot B, Kharroubi M, Metz R, Legros R, Rousset A (1991) Phys Status Solidi A 124:317
5. Vandenberghe RE, Brabers VAM, Robbrecht GG (1973) Phys Status Solidi A 16:K117
6. Vandenberghe RE, Robbrecht GG (1973) Mater Res Bull 8:571
7. Papavasiliou J, Avgouropoulos G, Ioannides T (2005) Catal Commun 6:497
8. Trari M, Topfer J, Dordor P, Grenier JC, Pouchard M, Doumerc JP (2005) J Solid State Chem 178:2751
9. Broemme ADD, Brabers VAM (1985) Solid State Ionics 16:171
10. Martin BE, Petric A (2007) J Phys Chem Solids 68:2262
11. Sinha APB, Sanjana NR, Biswas AB (1958) J Phys Chem 62:191
12. Miyahara S (1962) J Phys Soc Japan 17:181
13. Blasse G (1966) J Phys Chem Solids 27:383
14. Buhl R (1969) J Phys Chem Solids 30:805
15. Dubrovina IN, Balakirev VF, Antonov AV (2001) Inorg Mater 37:76
16. Dubrovina IN, Antonov AV, Balakirev VF, Chufarov GI (1981) Dokl Aakd Nauk SSSR 260:658
17. Kharroubi M, Gillot B, Legros R, Metz R, Vajpei AC, Rousset A (1991) J Less-Common Met 175:279
18. Driessens FCM, Rieck GD (1967) Z Anorg Allgem Chem 351:48
19. Gillot B, Buguet S, Kester E (1997) J Mater Chem 7:2513
20. Lenglet M, Huysser AD, Kasperek J, Bonnelle JP, Durr J (1985) Mater Res Bull 20:745
21. Vandenberghe RE, Robbrecht GG, Brabers VAM (1976) Phys Status Solidi A 34:583
22. Radhakrishnan NK, Biswas AB (1977) Phys Status Solidi A 44:45
23. Vandenberghe RE, Legrand E, Scheerilinck D, Brabers VAM (1976) Acta Cryst B32:2796
24. Cranswick LMD, Donaberger RL (2008) J Appl Crystallogr 41:1038
25. Cranswick LMD, Donaberger R, Swainson IP, Tun Z (2008) J Appl Crystallogr 41:373
26. Larson AC, Von Dreele RB (1994) General structure analysis system (GSAS). Los Alamos National Laboratory Report LAUR 86-748
27. Toby BH (2001) J Appl Crystallogr 34:210
28. Shannon RD (1976) Acta Crystallogr A 32:751
29. Dorris SE, Mason TO (1988) J Am Ceram Soc 71:379
30. Levin EM, Roth RS (1964) J Res NBS 68A:197
31. Maunders C, Martin BE, Wei P, Petric A, Botton GA (2008) Solid State Ionics 179:718
32. Zaslavskii AI, Plakhtii VP (1969) Sov Phys Solid State 11:3
33. Metz R (2000) J Mater Sci 35:4705. doi:10.1023/A:1004851022668